EIF4A3-Induced circARHGAP29 Promotes Aerobic Glycolysis in Docetaxel-Resistant Prostate Cancer through IGF2BP2/c-Myc/LDHA Signaling

Xingkang Jiang[1,2], Shanqi Guo[3], Shuo Wang[2], Yangyi Zhang[1], Haojie Chen[2], Yong Wang[1], Ranlu Liu[1], Yuanjie Niu[1], and Yong Xu[1]

ABSTRACT

Docetaxel-based chemotherapy is a standard-of-care treatment for metastatic prostate cancer, and chemoresistance remains a major challenge in clinical practice. Recent studies have demonstrated that circular RNAs (circRNA) play critical roles in the development and progression of prostate cancer. However, the biological roles and potential functions of circRNAs in mediating docetaxel-resistant prostate cancer have yet to be well elucidated. In this study, we analyzed the expression profiles of circRNAs in docetaxel-resistant and -sensitive prostate cancer cells through RNA sequencing and found that expression of *circARHGAP29* was significantly upregulated in docetaxel-resistant cell lines and clinical samples. Ectopic expression of *circARHGAP29* triggered docetaxel resistance and aerobic glycolysis in prostate cancer cells, which was reduced by silencing *circARHGAP29*. Moreover, eukaryotic initiation factor 4A3, which bound the back-spliced junction site and the downstream flanking sequence of *circARHGAP29*, induced cyclization and cytoplasmic export of *circARHGAP29*. *circARHGAP29* increased the stability of lactate dehydrogenase A (*LDHA*) mRNA by strengthening its interaction with insulin-like growth factor 2 mRNA-binding protein 2, leading to enhanced glycolytic metabolism. In addition, *circARHGAP29* interacted with and stabilized c-Myc mRNA and protein, which further increased LDHA expression by facilitating its transcription. These findings reveal the crucial function of *circARHGAP29* in prostate cancer glycolysis by increasing and stabilizing *LDHA* mRNA, providing a promising therapeutic target in docetaxel-resistant prostate cancer.

Significance: Upregulation of a novel circRNA, *circARHGAP29*, promotes docetaxel resistance and glycolytic metabolism, suggesting it could be a prognostic biomarker and therapeutic target in chemoresistant prostate cancer.

Introduction

Prostate cancer ranks as the most common malignancy and the second leading cause of cancer-related deaths among men, with an estimated 248,530 new cases and 34,130 deaths in 2021 in the United States (1). For patients with metastatic prostate cancer, the prognosis remains poor despite improvements in second-generation antiandrogens abiraterone acetate and enzalutamide. Docetaxel-based chemotherapy has been used as one of the first-line treatments for metastatic prostate cancer since 2004 (2). Although some patients with metastatic prostate cancer are responsive to docetaxel, there are still many patients who are intolerant or unresponsive to docetaxel. The development of docetaxel-resistant prostate cancer is a complex process that features genetic and epigenetic abnormalities (3, 4). Under these circumstances, a better comprehension of the mechanisms underlying the development of docetaxel resistance in patients with prostate cancer will represent a major step forward in optimizing patient outcomes.

Circular RNAs (circRNA), which are a newly discovered class of noncoding RNAs, are generated from back-splicing of pre-mRNA to form covalently closed transcripts (5). Previous studies have demonstrated that circRNAs can serve as miRNA sponges to affect translational processing. In addition, circRNAs can also interact with different proteins to form specific circRNA-protein complexes that subsequently influence the modes of action of associated proteins (5, 6). Notably, recent studies have described an emerging picture of circRNAs in prostate cancer, with tumor-promoting or inhibiting properties (7, 8). Nevertheless, the regulatory functions and complexities of circRNAs in modulating docetaxel resistance in prostate cancer have yet to be revealed.

Aerobic glycolysis, also termed the Warburg effect, is the most distinguishing difference between normal cells and malignant tumor cells. Cancer cells consume high levels of glucose, use enhanced glycolysis as the major energy metabolism pathway, and secrete high levels of lactic acid, where lactate dehydrogenase A (LDHA) is known as a key regulator of aerobic glycolysis, producing lactate from pyruvate (9, 10). Recent studies have demonstrated the roles of glucose metabolic reprogramming in chemoresistance among various cancers (11, 12). In 2020, Sun and colleagues revealed that Aurora-A regulated glucose metabolism to induce cisplatin resistance by participating in the SOX8/FOXK1 signaling axis in ovarian cancer cells (13). Zhou and colleagues reported that LDHA was a potential

[1]Department of Urology, Tianjin Institute of Urology, The Second Hospital of Tianjin Medical University, Tianjin, China. [2]The International Collaborative Laboratory for Biological Medicine of the Ministry of Education, The School of Medicine, Nankai University, Tianjin, China. [3]Department of Oncology, First Teaching Hospital of Tianjin University of Traditional Chinese Medicine, National Clinical Research Center for Chinese Medicine Acupuncture and Moxibustion, Tianjin, China.

Note: Supplementary data for this article are available at Cancer Research Online (http://cancerres.aacrjournals.org/).

X. Jiang and S. Guo contributed equally to this article.

Corresponding Author: Yong Xu, Department of Urology, Tianjin Institute of Urology, The Second Hospital of Tianjin Medical University, Pingjiang Road, Hexi District, Tianjin 300211, China. Phone: 8622-8832-6657; E-mail: xuyong8816@sina.com

Cancer Res 2022;82:831–45

doi: 10.1158/0008-5472.CAN-21-2988

therapeutic target for overcoming paclitaxel resistance and resensitizing breast cancer cells to paclitaxel (14). Besides, LDHA inhibitor catechin has been shown to be able to resensitize SNU620/5FU gastric cancer cells to 5-Fluorouracil (15). However, it is unclear whether circRNAs can mediate prostate cancer chemoresistance through anaerobic glycolysis, and what are the roles and potential mechanisms of circRNAs in this process.

In the current study, we discovered that *circARHGAP29*, a circRNA generated from the circularization of the *ARHGAP29* gene, was significantly upregulated in docetaxel-resistant prostate cancer cell lines and clinical samples. Subsequent studies showed that *circARHGAP29* could promote docetaxel resistance and glycolysis in prostate cancer *in vitro* and *in vivo*. We further identified that eukaryotic initiation factor 4A3 (EIF4A3) induced the cyclization and cytoplasmic export of *circARHGAP29* by binding with its back-spliced junction site and the downstream flanking sequence. In addition, *circARHGAP29* could bind to the insulin-like growth factor 2 mRNA-binding protein 2 (IGF2BP2) protein to stabilize *LDHA* mRNA. Moreover, *circARHGAP29* may stabilize the mRNA and protein levels of c-Myc, thus promoting LDHA expression at the transcriptional level. Taken together, our study delineated the novel roles of *circARHGAP29* in the regulation of glycolytic metabolism for docetaxel resistance, providing potential targets for the therapeutic intervention of prostate cancer.

Materials and Methods

Collection of clinical samples

This study was approved by the Ethics Committee of the Second Hospital of Tianjin Medical University, and written informed consent was obtained from all patients before the research started. The study was conducted in accordance with recognized ethical principles described in the Declaration of Helsinki. A total of 42 pairs of cancer tissues and paracancer samples were collected from patients with localized prostate cancer who underwent radical prostatectomy, as previously described (16). All samples were immediately snap-frozen in liquid nitrogen and stored at −80°C. Moreover, we collected blood samples from an additional 33 patients with metastatic prostate cancer who underwent at least 4 cycles of docetaxel-based chemotherapy at the Second Hospital of Tianjin Medical University from January 2020 to January 2021. Blood samples were centrifuged at 1500 × *g* for 10 minutes at 4°C, and the serum was collected and stored at −80°C for future analysis. Histologic and pathologic diagnoses were confirmed by at least two experienced histopathologists independently according to the criteria of the sixth edition TNM classification. The characteristics of patients with localized prostate cancer were listed in Supplementary Table S1.

Cell culture and treatment

The human prostate cancer cell lines PC3 and 22RV1 were purchased from the National Collection of Authenticated Cell Culture. The PC3 and 22RV1 cells were maintained in DMEM/F12 medium supplemented with 10% FBS (Biological Industries, Israel) and 1% penicillin-streptomycin in a humidified incubator at 37°C with 5% CO_2. Docetaxel-resistant cell lines were derived from the original parental cell lines by continuous exposure to docetaxel, as previously described (16, 17). Human 293T cells were cultured in DMEM supplemented with 10% FBS. Docetaxel, cycloheximide, bortezomib, and FX11 were purchased from MedChemExpress, and actinomycin D (ActD) was purchased from Sigma-Aldrich.

Cell growth, colony formation, and cytotoxicity

Cells were seeded in 96-well plates, and cell viability was evaluated with a Cell Counting Kit 8 (CCK-8, Dojindo). For the colony formation assay, cells were seeded in 6-well plates, and cultured colonies were stained with 0.1% crystal violet. In addition, cell proliferation was measured by EdU Incorporation Assays (Riobio). Briefly, cells seeded in 96-well plates were treated with docetaxel for 48 hours and labeled with 50 μmol/L EdU for an additional 2 hours. Then, the cells were fixed with 4% paraformaldehyde in PBS and stained with 1× Apollo medium. Finally, the cells were subjected to nuclear staining with DAPI for 30 minutes.

Glucose uptake, lactate production, and LDH activities

For the measurement of glucose consumption, lactate production, and LDH activities, cell supernatant was harvested and analyzed by a Glucose Assay Kit (Dojindo), a Lactate Assay Kit (Dojindo), and an LDHA Activities Kit (Abbkine) according to the manufacturer's instructions. In brief, a total of 2,000 cells were seeded in each well of a 96-well plate and incubated for 48 hours. After that, 20 μL of cell culture supernatant were transferred into a nonsterile 96-well plate and diluted with 180 μL ultrapure water. To detect the extracellular glucose content, we added 50 μL of diluted samples to 50 μL of glucose mixture. After 30 minutes of incubation at 37°C, the absorbance at 450 nm was measured on a plate reader. For the detection of lactate production, 20 μL of diluted samples and 80 μL lactate mixture were added into a clear 96-well plate. The plate was incubated for 30 minutes at 37°C in the dark before the absorbance at 450 nm was measured. To measure the LDH activities, we added 50 μL of diluted samples and 50 μL LDH mixture into a new 96-well plate. Then, we detected the absorbance at 450 nm before and after 30-minute incubation at 37°C.

RNA isolation, RNase R treatment, and qRT-PCR

Total RNA was isolated from cell lines and clinical samples using TRIeasy Reagent (Yeasen). In addition, nuclear and cytoplasmic RNA was extracted using a PARIS Kit (Thermo Fisher Scientific). For RNase R treatment, 1 μg of RNA was incubated for 20 minutes at 37°C with or without 2 U of RNase R (Geneseed). Reverse transcription was performed to synthesize cDNA using the circRNA qPCR Kit (Geneseed). Real-time PCR analyses were performed using Hieff SYBR Green Master Mix (Yeasen). The relative expression levels of circRNA and mRNA were calculated using the $2^{-\Delta\Delta C_t}$ method. β-Actin was used as an internal control to normalize the expression of target genes. Primer sequences are listed in Supplementary Table S2.

RNA sequencing

Total RNA was isolated from docetaxel-resistant PC3/DR and sensitive PC3 cells by TRIzol Reagent (Invitrogen). RNA quantification and quality assessment were performed by Qubit 3.0 and Agilent 2100 Bioanalyzer. Next, RiboZero rRNA Removal Kit was used to deplete rRNA following the manufacturer's protocols. The rRNA-depleted RNA samples were fragmented into small pieces randomly and synthesized cDNA with random primer. Besides, the AMPure XP Kit (Beckman Coulter) was used to purify with the PCR amplification products of cDNA. Then, the Illumina HiSeq 4000 system (Illumina) was used to collect sequencing data following the standard procedures by Geneseed. For circRNA expression analysis, the reads were mapped to the genome using STAR software, and DCC algorithm was used to identify the circRNA and to estimate the circRNA expression. Trimmed mean of M-values was used to normalize the gene expression. The differentially expressed genes were assessed by the Bioconductor package edgeR.

RNA stability assay

RNA stability was determined using ActD treatment. In short, cells were seeded in 6-well plates. At 80% confluence, cells were treated with 5 μg/mL of ActD for 0, 8, or 18 hours before RNA isolation. The *circARHGAP29* and LDHA mRNA levels were detected by the qRT-PCR assay.

Plasmids and transfection

To construct *circARHGAP29* overexpression (OE) plasmids, human *circARHGAP29* cDNA was synthesized and cloned into the pLC5-ciR vector (Geneseed). In addition, the full-length cDNAs of human EIF4A3, IGF2BP2, c-Myc, and their mutants were cloned into the CMV-MCS-3×Flag-PGK-Puro vector (Hanyin). siRNAs specific for *circARHGAP29*, EIF4A3, IGF2BP2, c-Myc, and LDHA were designed and synthesized by RiboBio. To knockdown(KD) the expression of *circARHGAP29*, oligonucleotides encoding short hairpin RNAs (shRNA) specific for *circARHGAP29* were cloned into the GV112 lentivirus vector (GeneChem). For transient transfection of siRNAs, we used Lipofectamine 2000 Reagent (Invitrogen). In addition, cells were infected by lentivirus in the presence of polybrene (8 μg/mL) and screened by 2 μg/mL of puromycin (Sigma-Aldrich) for 2 weeks to obtain stable cell lines. The sequences of shRNA and siRNAs used are listed in Supplementary Table S2.

RNA pulldown assay, silver staining, and mass spectrometry analysis

RNA pulldown assays were conducted using a Pierce Magnetic RNA-Protein Pull-Down Kit (Thermo Fisher Scientific) according to the manufacturer's protocol. Biotin-labeled probes targeting the junction sites of *circARHGAP29*, the upstream and downstream flanking sequences of *circARHGAP29*, and the *LDHA* 3′UTR sequence were synthesized by GenePharma. Cellular lysates were incubated with a biotin-labeled probe, and the protein samples were further identified by Western blot. Silver staining was performed using the Fast Silver Staining Kit (Beyotime) as described in the protocol, and the mass spectrometry analysis was performed by H-Wayen. Protein identification and quantification were accomplished using Proteome Discoverer Software 2.4 (Thermo Fisher Scientific).

Western blotting

Tissues and cells were lysed on ice with RIPA lysis buffer containing 1 × protease inhibitor cocktail (Sigma-Aldrich). Equal amounts of proteins were loaded into a 10% SDS-PAGE gel and transferred to nitrocellulose membranes. The membranes were incubated with primary antibodies against EIF4A3 (1:1,000, ProteinTech), IGF2BP2 (1:2,000, ProteinTech), c-Myc (1:1,000, Abcam), and LDHA (1:2,000, Santa Cruz Biotechnology) overnight at 4°C. Then, the membranes were further incubated with secondary antibodies for 1 hour at room temperature. Finally, the protein bands were detected using a Pierce ECL Western Blotting kit (Thermo Fisher Scientific) with an imaging system.

RNA immunoprecipitation

RNA immunoprecipitation (RIP) assays were performed with the Magna RIP RNA-Binding Protein Immunoprecipitation Kit (Millipore) according to the manufacturer's protocol. The coprecipitated RNA was examined using qRT-PCR with specific primers. The primer sequences are listed in Supplementary Table S2.

Dual-luciferase reporter assay

To evaluate the stability of LHDA mRNA, we constructed the LDHA wild-type (WT) 3′UTR and binding motif-mutated 3′UTR vector in PHY-811 plasmids (Hanyin). In brief, PC3 cells were seeded in 24-well plates at a density of 5×10^4 cells per well. Then, cells were cotransfected with the above WT or mutant luciferase reporter plasmids and the relevant siRNAs using the Lipofectamine 2000. After 48 hours, the luciferase activity was measured using a Dual-Luciferase Reporter Assay System according to the manufacturer's instructions (Promega). Firefly luciferase activity was normalized to the corresponding Renilla luciferase activity. To validate the transcription of LDHA by c-Myc, we cloned the LDHA promoter sequence from +0 to −2,000 into the PHY-803 vector (Hanyin). Subsequently, PHY-LDHA reporter plasmids and c-Myc expression plasmids were transferred together into PC3 cells, and the luciferase activities were measured by using a Dual-Luciferase Reporter Assay System.

FISH and immunofluorescence

A Cy3-labeled probe specific to *circARHGAP29* was designed and synthesized by RiboBio, and a FISH assay was performed using a Fluorescent *In Situ* Hybridization Kit (RiboBio). Briefly, cells were fixed with 4% paraformaldehyde and permeabilized with 0.3% Triton X-100 (Solarbio). Hybridization was performed at 37°C overnight in a dark, humid chamber. After being washed three times in saline sodium citrate buffer, the coverslips were sealed with parafilm containing DAPI. For immunofluorescence, cells were fixed and permeabilized accordingly. After washing twice with PBS, cells were blocked with 5% BSA for 30 minutes at 37°C and incubated with IGF2BP2 antibody overnight at 4°C. The next day, the cells were washed with PBS and then incubated with the corresponding secondary fluorescent antibody for 30 minutes at 37°C, followed by sealing with parafilm containing DAPI. Fluorescent images were acquired using a confocal laser scanning microscope (Olympus).

Chromatin immunoprecipitation

Chromatin immunoprecipitation (ChIP) assays were performed using a ChIP Assay Kit (Millipore) according to the manufacturer's instructions. Briefly, cells were fixed with 1% formaldehyde for 10 minutes at room temperature and washed three times with cold PBS. Fixed cells were resuspended in lysis buffer and then subjected to sonication to shear DNA into fragments with lengths between 200 and 1,000 bp. After centrifugation, a small aliquot of chromatin was saved as an input control, and the rest was diluted in dilution buffer. The diluted chromatin was incubated with 1 μg of the corresponding antibody or normal immunoglobulin G. Immunoprecipitated DNA was purified and then analyzed by qRT-PCR. The antibodies used were anti–c-Myc (Abcam) and normal IgG (ProteinTech). The primer sequences are listed in Supplementary Table S2.

Tumor xenograft model

All animals were housed according to institutional guidelines and experiments were approved by the Animal Care Committee of Tianjin Medical University. Six-week-old male BALB/c nude mice were purchased from HFK Biosciences and preserved in an SPF-grade animal laboratory. Twenty-four nude mice were randomly divided into four groups, and a total of 5×10^6 cells were injected into the left flanks of nude mice subcutaneously. For drug treatment, mice were treated with or without docetaxel (5-mg/kg body weight) via intraperitoneal injection twice per week for 2 weeks. The tumor volume was measured every 3 days, and the final weight was recorded after

sacrifice. Tumor volumes were calculated as length × width^2 × 0.5. After 4 weeks, all mice were sacrificed, and the tumors were harvested and weighed.

Histology and IHC

Tumor tissues were fixed in 4% paraformaldehyde and embedded in paraffin. Sections were then processed for hematoxylin and eosin (H&E) and IHC. Primary antibodies specific for Ki-67 (1:5,000, ProteinTech), c-Myc (1:500, ProteinTech), and LDHA (1:5,000, Santa Cruz Biotechnology) were used. All images were recorded with an Olympus BX-51 light microscope.

Statistical analysis

All statistical analyses were performed using Prism 8.0 (GraphPad Software Inc.). Data were shown as the mean ± SD. The significance of intergroup differences was estimated with Student *t* test or one-way ANOVA. Correlations were analyzed by Pearson correlation test. All results were reproduced across triplicate experiments. Statistical significance was considered to be indicated by $P < 0.05$.

Ethics approval and consent to participate

The current study was approved by the Ethics Committee of the Second Hospital of Tianjin Medical University (KY2018K028).

Results

Elevated expression of circARHGAP29 in docetaxel-resistant prostate cancer cells and clinical samples

To explore the specific role and possible mechanisms of circRNA in docetaxel-resistant prostate cancer, we established two docetaxel-resistant prostate cancer cell lines as previously described (13, 14). Cell viability and colony formation verified chemoresistance (Supplementary Fig. S1A–S1D). Subsequently, we performed an RNA sequencing (RNA-seq) of ribosomal RNA-depleted total RNA, and the expression levels of circRNA transcripts varied between docetaxel-resistant PC3/DR cells and counterpart PC3 cells. Among the differentially expressed circRNAs, 52 were upregulated and 21 were downregulated in docetaxel-resistant cells relative to sensitive cells (fold change > 1.5 and *P* value <0.05; **Fig. 1A** and **B**). Subsequently, we selected the top 10 upregulated circRNAs according to the inclusion criteria for further validation by qRT-PCR (Supplementary Fig. S1E). *Hsa_circ_0003310* (termed *circARHGAP29*), which was expressed at the highest level among these circRNAs, attracted our attention (Supplementary Fig. S1F). Consistent with the RNA-seq results, *circARHGAP29* was remarkably upregulated circRNA in docetaxel-resistant prostate cancer cells compared with sensitive cell lines (**Fig. 1C**). However, the expression of linear *ARHGAP29* mRNA showed no significant difference between docetaxel-resistant cell lines and docetaxel-sensitive cells (Supplementary Fig. S1G and S1H). Using bioinformatic methods (circBase and circBank), we found that *circARHGAP29* was a 372-nt circRNA derived from exons 21 and 22 within the ARHGAP29 locus, the back-spliced junction point of which was amplified with divergent primers and validated by Sanger sequencing (**Fig. 1D**). To further confirm the circular characteristics of *circARHGAP29*, the head-to-tail splicing of endogenous *circARHGAP29* was assessed by qRT-PCR with convergent and divergent primers. As expected, *circARHGAP29* could be amplified by divergent primers in cDNA but not genomic DNA (**Fig. 1E**). Resistance to digestion with RNase R exonuclease also confirmed that *circARHGAP29* harbored a circRNA structure (**Fig. 1F**). Moreover, *circARHGAP29* transcripts were more stable than ARHGAP29 and GAPDH mRNA upon treatment with ActD (**Fig. 1G**). In addition, we further detected the subcellular location of *circARHGAP29* by nuclear/cytoplasmic fractionation assay and FISH assay. The results showed that *circARHGAP29* was predominantly located in the cytoplasm of PC3/DR cells compared with PC3 cells (**Fig. 1H** and **I**). In addition, the expression of *circARHGAP29* was upregulated in human primary prostate cancer tissues compared with paired adjacent samples (**Fig. 1J**). The increased *circARHAP29* was especially detected in patients with prostate cancer with higher Gleason grade and in more advanced clinical tumor stages. However, *circARHAP29* expression showed no correlation with age, prostate-specific antigen level, and lymph-nodes status (Supplementary Table S1). Moreover, we next explored whether *circARHGAP29* could be used to predict docetaxel response in patients with metastatic prostate cancer. As shown in **Fig. 1K**, the average level of *circARHGAP29* in pretherapy plasma was higher in patients who suffered from progressive disease (PD) during docetaxel therapy than in those without PD. Therefore, these findings indicated that *circARHGAP29* might contribute to the docetaxel resistance in prostate cancer.

circARHGAP29 promotes docetaxel resistance in prostate cancer cells

To explore the functional role of *circARHGAP29* in docetaxel-resistant prostate cancer cells, we constructed and transfected *circARHGAP29* plasmid into PC3 cells and 22RV1 cells, and the efficacy was further verified through qRT-PCR assay (**Fig. 2A**; Supplementary Fig. S2A). Subsequently, cell viability was evaluated with CCK-8 and EdU assays, which indicated that *circARHGAP29* promoted docetaxel resistance of both PC3 cells (**Fig. 2B** and **C**) and 22RV1 cells (Supplementary Fig. S2B). Cell colony formation was also maintained in the presence of docetaxel when prostate cancer cells were transfected with *circARHGAP29* plasmids (**Fig. 2D**; Supplementary Fig. S2C). In addition, we designed two *circARHGAP29* siRNAs that specifically targeted their back-splicing sites (Supplementary Fig. S2D). The KD efficiency was further verified by qRT-PCR assay, and siRNA #1 provided the most effective KD (**Fig. 2E**). However, there was no significant difference in *ARHGAP29* mRNA expression in *circARHGAP29*-KD cells (Supplementary Fig. S2E). Subsequent cell viability and colony formation assays also confirmed that downregulation of *circARHGAP29* by using two siRNA molecules reduced the sensitivity of cells to docetaxel (**Fig. 2F–H**; Supplementary Fig. S2F and S2G). To determine whether *circARHGAP29* is an alternative therapeutic target that could improve docetaxel-based therapy in docetaxel-resistant cancers, we constructed *circARHGAP29* shRNA using the sequence of siRNA #1 to stably knock-down the expression of *circARHGAP29* in PC3/DR cells. After that, PC3/DR cells stably transfected with shRNA-*circARHGAP29* or control vector were injected into BALB/c nude mice subcutaneously, followed by intraperitoneal DMSO and docetaxel treatment (Supplementary Fig. S2H). Supporting the results obtained *in vitro*, as shown in **Fig. 2I–K**, KD of *circARHGAP29* strikingly decreased the tumor volumes and weights and weakened the docetaxel resistance of PC3/DR cells. Importantly, H&E and IHC analysis revealed an obvious reduction of tumor sizes and the inhibition of Ki-67 in the *circARHGAP29*-KD group upon docetaxel treatment compared with the control group (**Fig. 2L**). Together, these findings indicated that *circARHGAP29* could promote tumor growth and was essential for the sensitivity of prostate cancer cells to docetaxel chemotherapy.

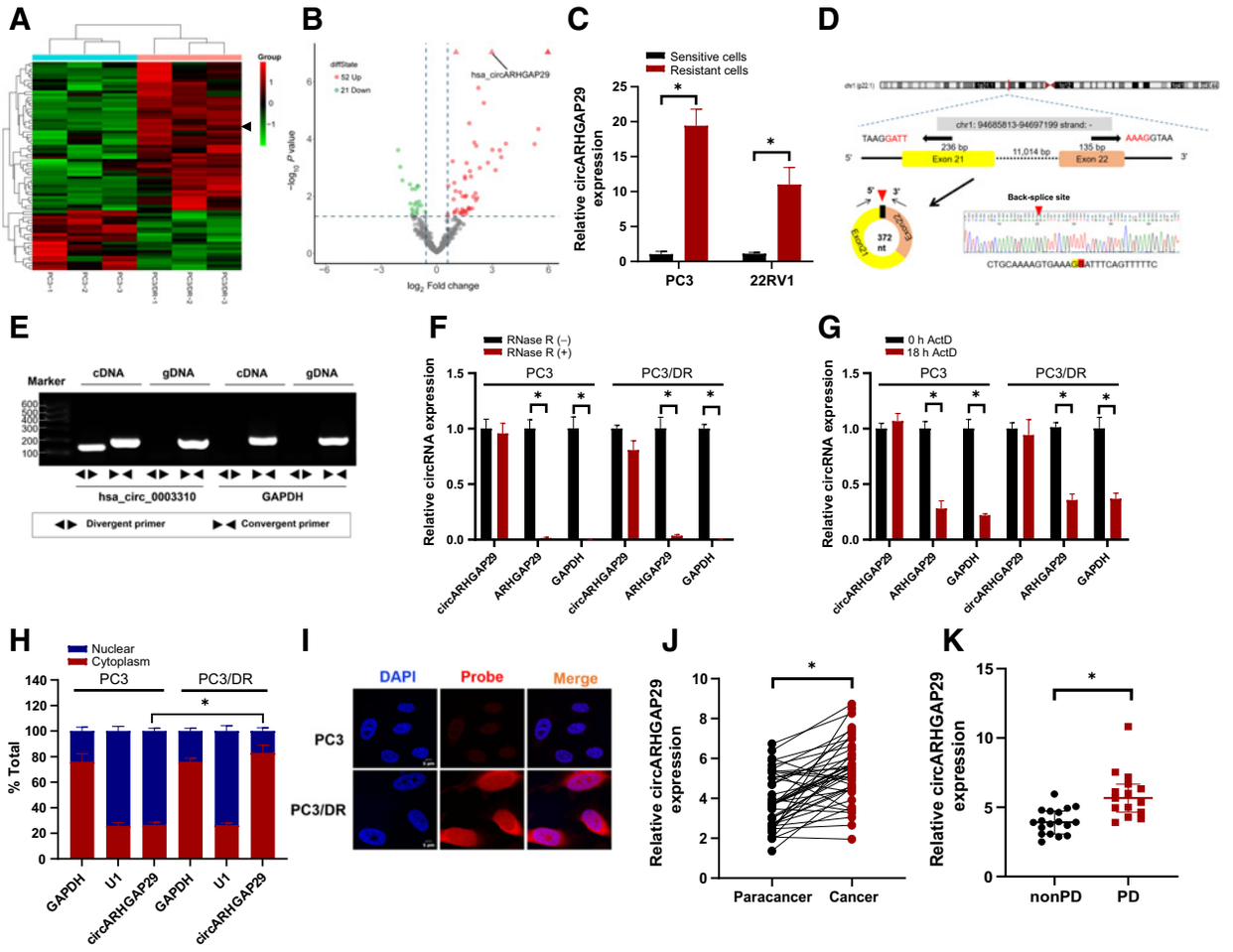

Figure 1.

circARHGAP29 is verified and characterized in docetaxel-resistant prostate cancer cells and clinical samples. **A** and **B,** Heatmap and volcano plot represent the differentially expressed circRNAs in docetaxel-resistant PC3/DR cells and counterpart PC3 cells. The red and green represent the upregulated and downregulated circRNAs. Arrow, *hsa_circ_0003310* (termed *circARHGAP29*). **C,** The expression of *circARHGAP29* was detected by qRT-PCR in docetaxel-resistant prostate cancer cells (PC3/DR and 22RV1/DR) and sensitive cell lines (PC3 and 22RV1). **D,** Schematic illustration of *circARHGAP29* formation via the circularization from exons 21 to exon 22 in the ARHGAP29 gene. The back-splice junction sequences were confirmed by Sanger sequencing. **E,** The existence of *circARHGAP29* from cDNA and gDNA in PC3 cells was detected by RT-PCR with the divergent and convergent primers. GAPDH was used as a linear control. **F** and **G,** The relative expression of *circARHGAP29*, ARHGAP29, and GAPDH was measured by qRT-PCR after treatment with ActD and RNase R. **H,** Nuclear–cytoplasmic fractionation assay was used to assess the intracellular location of *circARHGAP29* in PC3/DR and PC3 cells. U1 was considered as a nuclear control and GAPDH was used as a cytoplasmic protein control. **I,** The subcellular location of *circARHGAP29* was also evaluated by FISH assays. Nuclei were stained with DAPI. **J,** The relative expression of *circARHGAP29* was detected by qRT-PCR in 42 pairs of primary prostate cancer tissues and paracancer samples. **K,** qRT-PCR analysis of *circARHGAP29* in the pretherapy plasma of patients with prostate cancer with PD ($n = 15$) or nonPD ($n = 18$) during docetaxel therapy. The data are presented as the mean ± SD of at least three independent experiments. *, $P < 0.05$.

EIF4A3 induces the cyclization and cytoplasmic export of circARHGAP29

Previous studies demonstrated that some RNA-binding proteins (RBP) can bind to circRNA flanking intron sequences, playing an important role in the generation of circRNAs (18). Therefore, to further explore how *circARHGAP29* was upregulated in docetaxel-resistant prostate cancer, we searched the circInteractome and circAltas databases to predict potential RBP sites in the flanking regions of *circARHGAP29*, and found that EIF4A3 had the most possible binding sites (Supplementary Fig. S3A and S3B). To verify the ability of EIF4A3 to bind to *circARHGAP29* flanking sequences, we performed an RNA pulldown assay using specific biotin-labeled probes. As illustrated in **Fig. 3A–C**, EIF4A3 could bind to both the back-spliced junction site and the downstream flanking sequence of *circARHGAP29*, but not the upstream sequences. In addition, the RIP assay also identified that endogenous EIF4A3 could bind with the back-spliced junction site (named b) and three downstream putative binding sites (named c, d, and e) but not the upstream sites (named a; **Fig. 3D**). By performing FISH-IF assays, we confirmed that the cytoplasmic expression levels of EIF4A3 and *circARHGAP29* were increased in PD3/DR cells compared with PC3 cells (**Fig. 3E**). Previous studies have shown that EIF4A3 could mediate RNA splicing and the

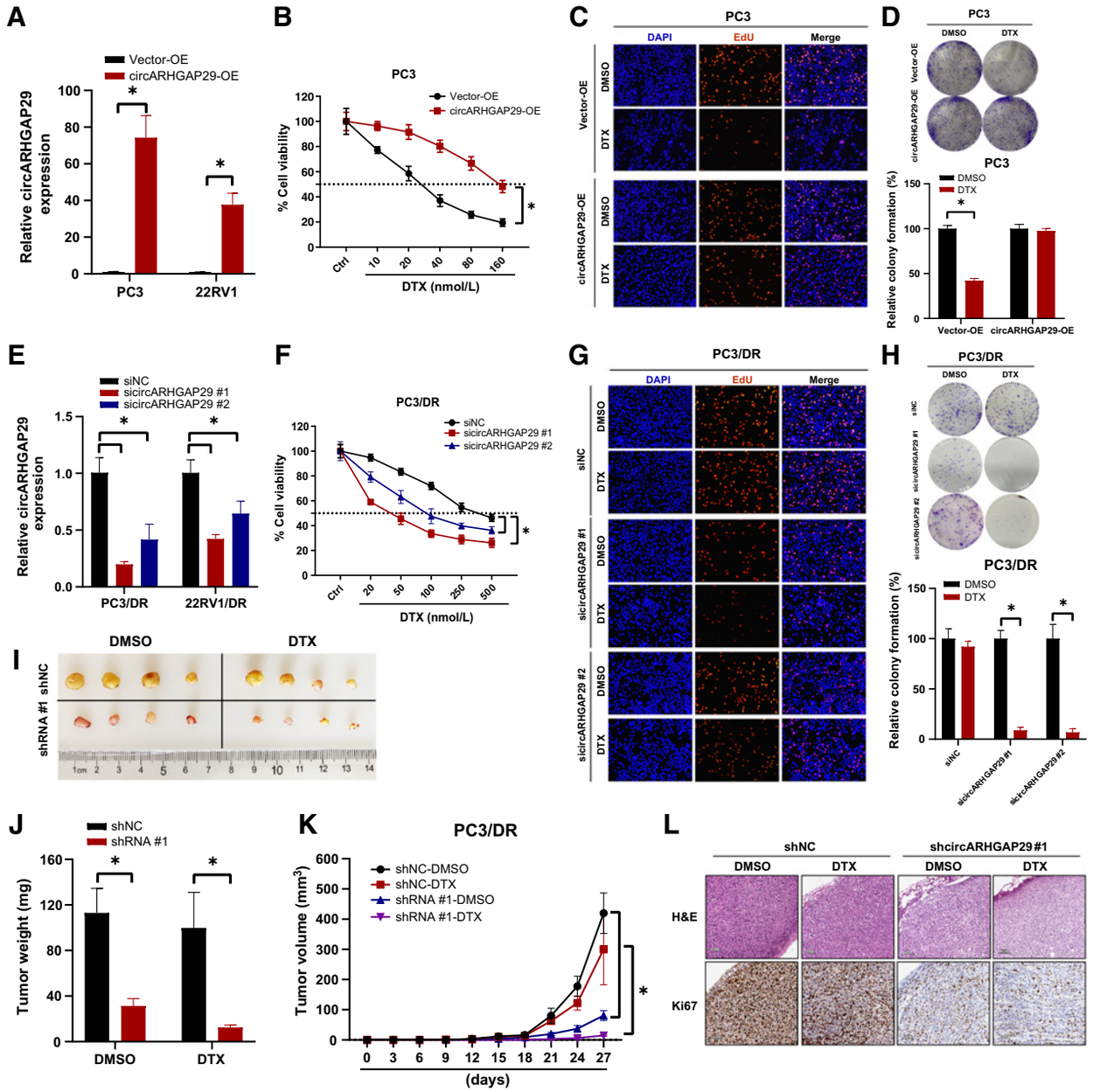

Figure 2.

circARHGAP29 increases cell proliferation and docetaxel resistance in prostate cancer cells. **A,** The efficiency of *circARHGAP29* OE in PC3 and 22RV1 cells was verified by qRT-PCR. **B,** Cells were treated with different dosages of docetaxel (concentration of 0, 10, 20, 40, 80, and 160 nmol/L) for 72 hours, and cell viability was evaluated by a CCK-8 assay. **C** and **D,** EdU and colony formation assays were used to assess cell survival in *circARHGAP29*-OE PC3 cells after 20 nmol/L docetaxel treatment. **E,** The relative expression of *circARHGAP29* was detected by qRT-PCR in PC3/DR and 22RV1/DR cells after transfection with *circARHGAP29* siRNA and control siRNA. **F–H,** CCK-8, EdU, and colony formation assays were used to evaluate the cell growth and docetaxel resistance in PC3/DR cells after transfection with si*circARHGAP29* #1 or #2. **I,** Representative images of xenograft tumors of *circARHGAP29*-KD PC3/DR group (shRNA #1) and their control group (shNC) after being treated with either docetaxel or DMSO. **J** and **K,** The tumor growth curves were drawn and tumor weight was measured. **L,** H&E staining was performed to evaluate tissue morphology, and IHC was performed to evaluate Ki-67 expression in the *circARHGAP29*-KD groups and their control groups under docetaxel treatment. The data are presented as the means ± SD of at least three independent experiments. *, $P < 0.05$. DTX, docetaxel.

nuclear export of spliced RNA (19). Thus, we speculated that EIF4A3 could also promote the cyclization and cytoplasmic export of *circARHGAP29*. As shown in **Fig. 3F**, inhibition of EIF4A3 led to a reduction of *circARHGAP29*. Interestingly, we observed a clear reduction of cytoplasmic *circARHGAP29* levels in PC3/DR and 22RV1/DR cells upon EIF4A3 KDknockdown (**Fig. 3G** and **H**). To further elucidate the binding sites of EIF4A3 in the *circARHGAP29* pre-mRNA transcript, we searched by the catRAPID algorithm and

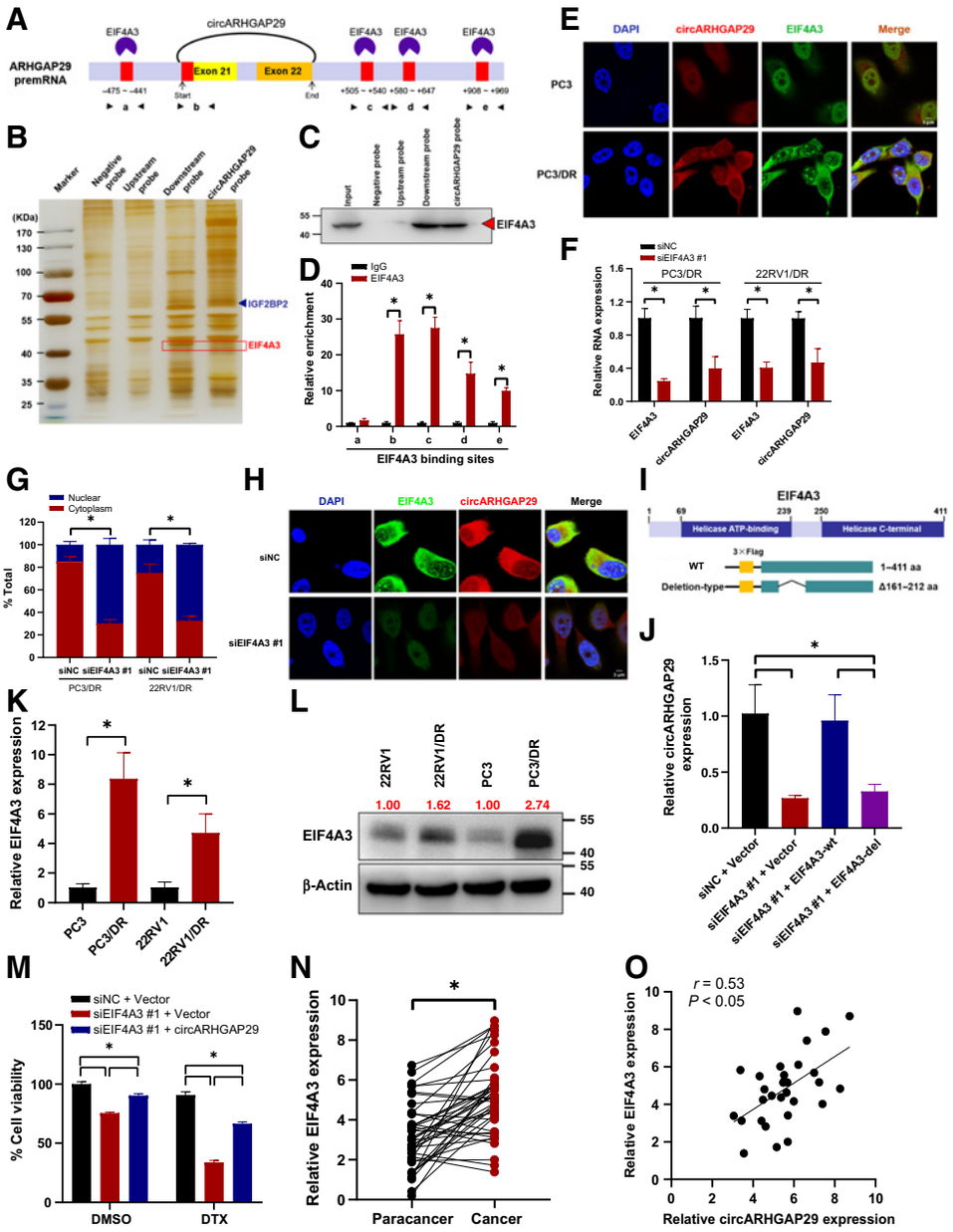

Figure 3.

The RNA binding protein EIF4A3 regulates the expression of circARHGAP29. **A,** The binding sites for EIF4A3 in the flanking sequences of ARHGAP29 mRNA transcript were predicted using CircInteractome. **B,** The RNA-protein pulldown assay and fast silver staining were performed to illustrate the possible binding proteins in the *circARHGAP29* flanking sequences. Upstream biotin-labeled probe contains the predicted upstream binding sequences (−605 to −131), *circARHGAP29* probe contains the back-spliced junction site, and downstream probe contains three possible downstream sequences (+501 to +996). **C,** Western blot was used to verify the interaction between EIF4A3 and *circARHGAP29* flanking sequences. **D,** RIP assay was performed to identify the putative binding sites of EIF4A3 in the *circARHGAP29* pre-mRNA transcript. **E,** The subcellular location of EIF4A3 and *circARHGAP29* in PC3/DR and PC3 cells was detected by immunofluorescence and FISH assay. Nuclei were stained with DAPI. **F,** The relative expression of EIF4A3 and *circARHGAP29* was evaluated by qRT-PCR in PC3/DR and 22RV1/DR cells after transfection with siEIF4A3 #1 and control siRNA. **G** and **H,** Nuclear–cytoplasmic fractionation and FISH-IF assays were used to evaluate the cytoplasmic export of *circARHGAP29* in PC3/DR and 22RV1/DR cells upon EIF4A3 KD. **I,** The illustration of the WT and deletion mutant (Δ161–212 aa) expression plasmids for EIF4A3. **J,** The relative expression of *circARHGAP29* was detected in EIF4A3-KD PC3/DR cells after transfection with EIF4A3 WT or deletion mutant plasmids by qRT-PCR. **K** and **L,** The mRNA and protein levels of EIF4A3 were evaluated by qRT-PCR and Western blot in docetaxel-resistant prostate cancer cells (PC3/DR and 22RV1/DR) compared with sensitive cell lines (PC3 and 22RV1). ImageJ was used to compare the density of bands on Western blot. **M,** The cell viability was evaluated by CCK-8 assay in PC3/DR cells transfected with EIF4A3 siRNA #1 and/or *circARHGAP29* expression plasmids upon docetaxel (DTX; 50 nmol/L) or DMSO treatment. **N,** The expression of EIF4A3 was detected by qRT-PCR in primary prostate cancer samples and their paracancer tissues. **O,** The correlation between *EIF4A3* and *circARHGAP29* expression in clinical prostate cancer samples was assessed by the Spearman correlation analysis. The data are presented as the means ± SD of at least three independent experiments. *, $P < 0.05$.

identified the 161–212 aa peptide of EIF4A3 as a possible interaction region (Supplementary Fig. S3C and S3D). Consequently, we constructed WT and deletion mutant (Δ161–212 aa) expression plasmids for EIF4A3 (**Fig. 3I**). Ectopic expression of WT EIF4A3, but not the deletion form, restrained the EIF4A3-KDknockdown–induced inhibition of *circARHGAP29* in the PC3/DR cells (**Fig. 3J**). In contrast, silencing *circARHGAP29* did not change the EIF4A3 mRNA and protein levels (Supplementary Fig. S3E and S3F). As expected, we found that the mRNA and protein levels of EIF4A3 were upregulated in docetaxel-resistant cell lines (**Fig. 3K** and **L**). CCK-8 assay showed that silencing of EIF4A3 increased the cytotoxicity of docetaxel in PC3/DR cells, whereas ectopic expression of *circARHGAP29* restrained the docetaxel-resistant phenotype (**Fig. 3M**). In addition, elevated EIF4A3 expression was also identified in primary prostate cancer samples compared with their adjacent tissues, and there was a positive correlation between *circARHGAP29* and EIF4A3 in prostate cancer samples (**Fig. 3N** and **O**). Moreover, the GEPIA database indicated that the expression level of EIF4A3 was markedly increased in prostate cancer samples compared with normal tissues, and patients with high EIF4A3 expression had a shorter disease-free survival time than those with low expression (Supplementary Fig. S3G–S3I). Taken together, EIF4A3 induces the cyclization and cytoplasmic export of *circARHGAP29* by the 161–212 aa binding sites of EIF4A3 and the back-spliced junction site and the downstream flanking sequences of *circARHGAP29*.

circARHGAP29 interacts with the IGF2BP2 protein through the KH3–4 domain

After database analysis (circRNADb), we found that *circARHGAP29* does not have an internal ribosome entry site and open reading frame regions, meaning that *circARHGAP29* does not have protein- or peptide-encoding features (Supplementary Fig. S4A). To determine whether cytoplasm-localized *circARHGAP29* functions as a miRNA sponge, we analyzed argonaute 2 (Ago2) cross-linking immunoprecipitation and high throughput sequencing (CLIP-seq) data and found that *circARHGAP29* did not bind to Ago2, which was supported by the Ago2 reciprocal RNA pulldown and RIP assay (Supplementary Fig. S4B and S4C). Thus, we ruled out the function of *circARHGAP29* as a miRNA sponge in prostate cancer progression. Given that *circARHGAP29* is mainly located in the cytoplasm, we next performed an RNA pulldown assay to explore its protein-binding role using biotinylated probes targeting the *circARHGAP29* back-spliced sequence. After silver staining and mass spectrometry analysis, a major differential band precipitated in PC3/DR lysates was identified to be the IGF2BP2 protein (**Figs. 3A** and **4A**), which was further predicted by the circAltas database (Supplementary Fig. S4B). Subsequently, the interaction between endogenous IGF2BP2 and *circARHGAP29* was further validated by probing the immunoprecipitates by anti-IGF2BP2 antibody and RIP assay (**Fig. 4B** and **C**). FISH-IF assay identified the colocalization of endogenous *circARHGAP29* and IGF2BP2 in the cytoplasm, indicating that *circARHGAP29*/IGF2BP2 forms an RNA-protein complex in the cytoplasm (**Fig. 4D**). Consistent with the elevated expression of *circARHGAP29*, qRT-PCR and Western blot assay revealed that PC3/DR and 22RV1/DR cells had higher expression levels of IGF2BP2 than control cells (**Fig. 4E** and **F**). Moreover, the serum IGF2BP2 level was slightly upregulated in docetaxel-resistant patients with prostate cancer compared with those of docetaxel-sensitive patients with prostate cancer (**Fig. 4G**). However, either KD or OE of *circARHGAP29* did not alter IGF2BP2 expression levels, indicating that *circARHGAP29* was not involved in the posttranslational regulation of IGF2BP2 (Supplementary Fig. S4D). To delineate which domain of IGF2BP2 contributes to the interaction with *circARHGAP29*, we searched by the catRAPID algorithm and found that the 476–527 aa peptide of IGF2BP2 was the possible interaction region (**Fig. 4H**; Supplementary Fig. S4E). Consequently, an anti-Flag RIP assay revealed that removal of the binding sites (aa476–527) of IGF2BP2 abolished its association with *circARHGAP29*, suggesting that the region between KH3 and KH4 of IGF2BP2 specifically bound to *circARHGAP29* (**Fig. 4I**). CCK-8 assay showed that inhibition of IGF2BP2 increased the cytotoxicity of docetaxel in PC3/DR cells, while ectopic expression of IGF2BP2-WT restrained the above phenotype (**Fig. 4J**). In summary, these results showed that *circARHGAP29*/IGF2BP2 formed an RNA-protein complex through the region linking KH3 and KH4 domains of IGF2BP2 in docetaxel-resistant prostate cancer cells.

circARHGAP29/IGF2BP2 promotes the stability of LDHA mRNA levels

IGF2BP2 has been suggested as an m6A reader governing mRNA stability (20–22). We assumed that *circARHGAP29* may regulate mRNA stability through its interaction with IGF2BP2. To confirm this hypothesis, we performed RNA-seq analyses in *circARHGAP29*-KD PC3/DR cells. A total of 195 mRNAs showed a significant decrease in mRNA levels upon *circARHGAP29* silencing (fold change < 0.6; **Fig. 5A**). It has been reported that IGF2BP2 preferentially binds to the 3′UTRs of target mRNAs (21, 22). Therefore, among 195 downregulated mRNAs, we screened IGF2BP2-binding 3′UTRs from published RBP CLIP-Seq data sets (starBase) and identified 5 mRNAs bound by IGF2BP2 (**Fig. 5B**). After screening the literature, two chemoresistance-related genes (LDHA and c-Myc) were identified as potential targets of *circARHGAP29* and IGF2BP2. Subsequently, we found the mRNA and protein level of LDHA were decreased upon *circARHGAP29* or IGF2BP2 KD in PC3/DR and 22RV1/DR cells (**Fig. 5C** and **D**). Since previous study illustrated that IGF2BP proteins preferentially bind to the "UGGAC" consensus sequence in the 3′UTRs, we therefore predicted a protein-RNA interaction between IGF2BP2 and LDHA by bioinformatic analysis (starBase; **Fig. 5E**; Supplementary Fig. S5A and S5B; ref. 22). Consequently, we carried out the RNA pulldown assays using a biotin-labeled 3′UTR fragment of *LDHA* containing the predicted binding motif. The results showed that a significant enrichment of IGF2BP2 protein binds to the *LDHA* 3′UTR sequence compared with the negative control (**Fig. 5F**). To further investigate whether IGF2BP2 is indispensable for *LDHA* mRNA stabilization, we performed an RIP assay using an antibody specifically against Flag. qRT-PCR results revealed that *LDHA* mRNA were significantly enriched in Flag-coprecipitated RNA fragments of IGF2BP2-WT cells compared with those of IGF2BP2-Del cells (**Fig. 5G**). Besides, RIP assays also identified that KD of *circARHGAP29* significantly diminished the IGF2BP2/*LDHA* RNA-protein interaction in PC3/DR cells, whereas ectopic OE of *circARHGAP29* in PC3 cells significantly increased the enrichment of *LDHA* in IGF2BP2 immunoprecipitated fractions (**Fig. 5H**). The above results together demonstrated a specific association between *circARHGAP29*/IGF2BP2 and *LDHA* mRNA. To further assess the direct binding of IGF2BP2 on the predicted sequence of *LDHA* 3′UTR regions, we constructed luciferase reporter plasmids containing WT LDHA-3′UTR (LDHA-WT) or mutant 3′UTR (LDHA-Mut). KD of *circARHGAP29* or IGF2BP2 dramatically inhibited the luciferase activity of LDHA-WT, but not that of LDHA-Mut (**Fig. 5I**). Moreover, we also performed RNA stability assays to validate the effects of *circARHGAP29*/IGF2BP2 on the mRNA stability of LDHA through the above-described mechanisms.

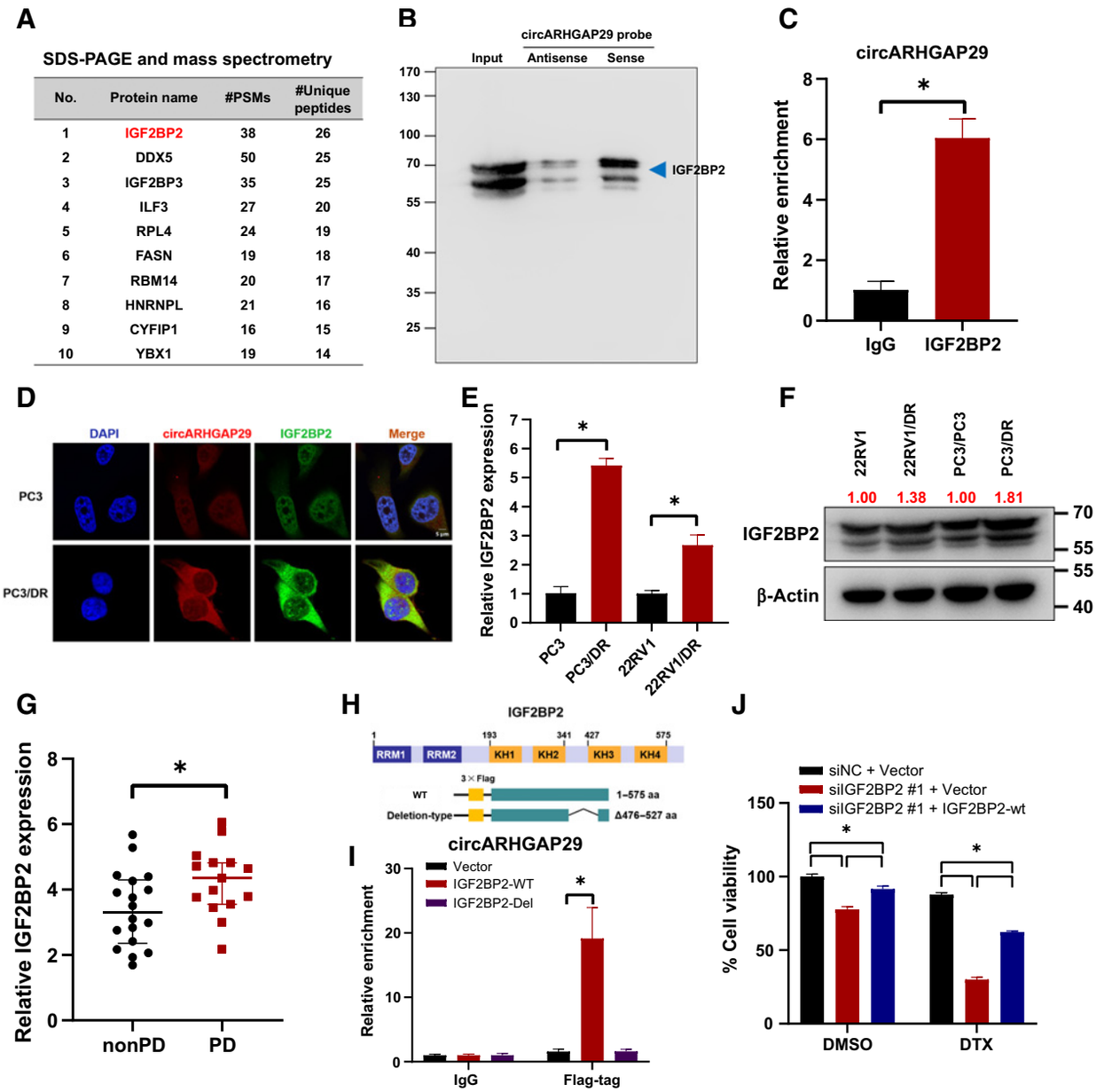

Figure 4.

circARHGAP29 interacts with the IGF2BP2 protein through the KH3–4 domain. **A,** List of main *circARHGAP29*-related RBPs after mass spectrometry analysis and IGF2BP2 ranks at the top. **B,** Western blot was used to verify the association between *circARHGAP29* and IGF2BP2 using biotinylated probes targeting the *circARHGAP29* back-spliced sequence. **C,** RIP assays show the association of IGF2BP2 and *circARHGAP29*. IgG was used as the negative control. **D,** The subcellular location of IGF2BP2 and *circARHGAP29* in PC3/DR and PC3 cells was evaluated by immunofluorescence and FISH assay. Nuclei were stained with DAPI. **E** and **F,** The mRNA and protein levels of IGF2BP2 were detected by qRT-PCR and Western blot in docetaxel-resistant prostate cancer cells (PC3/DR and 22RV1/DR) compared with sensitive cell lines (PC3 and 22RV1). The bands of Western blot were quantified by ImageJ. **G,** The serum IGF2BP2 level was evaluated by qRT-PCR in patients with metastatic prostate cancer with PD ($n = 15$) or nonPD ($n = 18$) after 4 cycles of docetaxel chemotherapy. **H,** The schematic structures showing the WT and deletion mutant (Del; Δ476–527 aa) expression plasmids for IGF2BP2. **I,** Relative enrichment representing *circARHGAP29* levels associated with Flag-tag plasmids of IGF2BP2 WT or deletion mutation relative to the input control. **J,** The cell viability was detected by CCK-8 assay in PC3/DR cells after transfection with IGF2BP2 siRNA #1 and/or IGF2BP2-WT expression plasmids upon docetaxel (DTX; 50 nmol/L) or DMSO treatment. The data are presented as the mean ± SD of at least three independent experiments. *, $P < 0.05$.

As shown in **Fig. 5J**, inhibition of *circARHGAP29* or IGF2BP2 greatly decreased the stability of LDHA mRNA after 8 hours of ActD treatment. In contrast, we also found that ectopic expression of IGF2BP2 WT, but not the deletion form, restrained the *circARHGAP29*-KD–induced suppression of LDHA levels (**Fig. 5K**). These findings demonstrate that *circARHGAP29* enhances the mRNA stability of LDHA although the formation of a *circARHGAP29*/IGF2BP2/*LDHA* RNA-protein ternary complex.

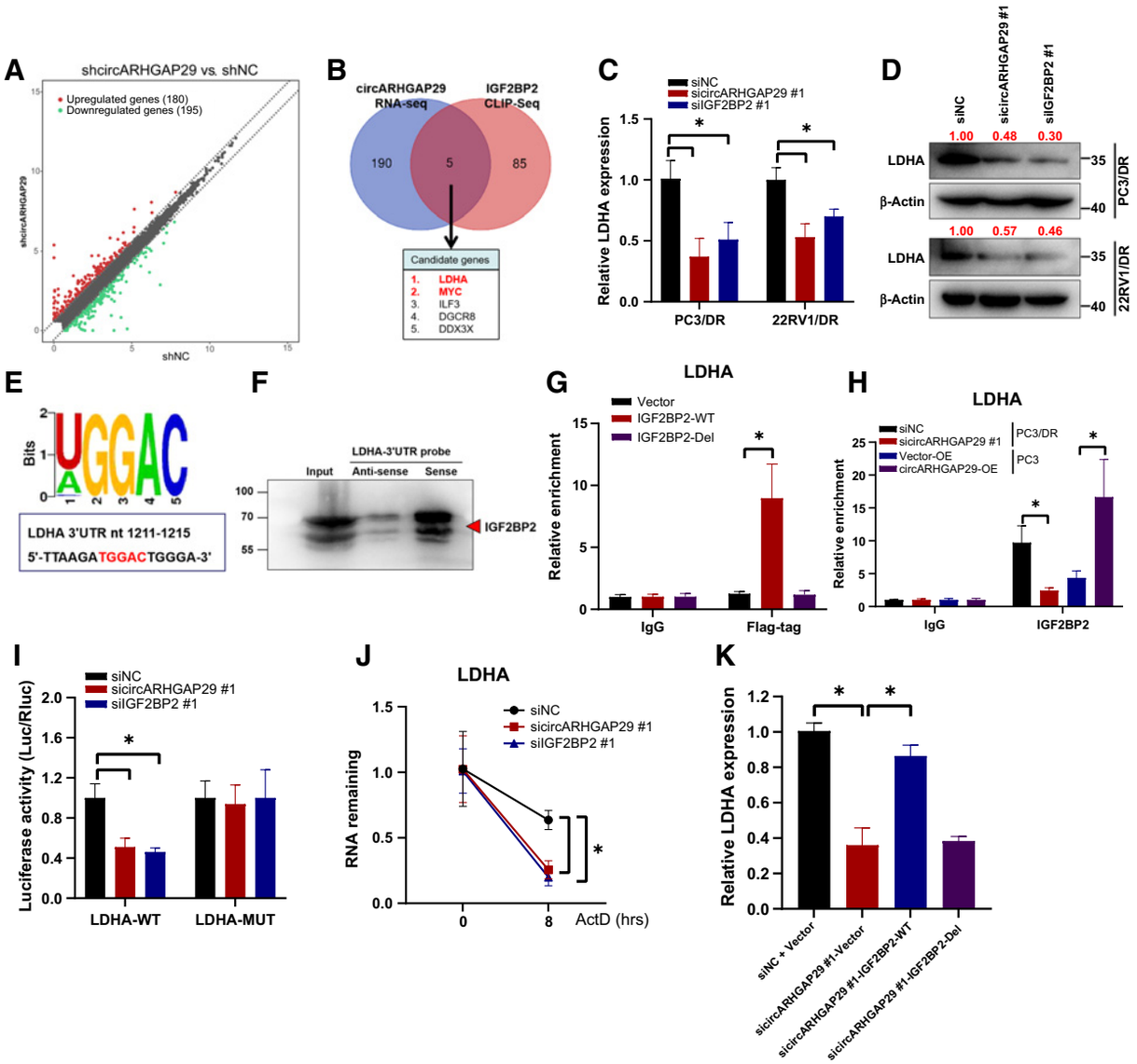

Figure 5.

circARHGAP29/IGF2BP2 promotes the stability of LDHA mRNA levels. **A,** The scatter plot shows 195 genes were downregulated in PC3/DR cells after *circARHGAP29* KD. **B,** Venn diagram showing the possible target genes of both *circARHGAP29* and IGF2BP2 from RNA-seq data and CLIP-Seq data sets. **C** and **D,** The mRNA and protein levels of LDHA were detected by qRT-PCR and Western blot in PC3/DR and 22RV1/DR cells after *circARHGAP29* or IGF2BP2 KD. ImageJ was used to compare the density of bands on Western blot. **E,** Predicted binding motif of IGF2BP2 on 3′UTR of LDHA mRNA from Starbase website. **F,** RNA pulldown assay and Western blot were used to verify the association between IGF2BP2 protein and LDHA 3′UTR regions. **G,** RIP assay was performed in PC3 cells using anti-IgG and anti-Flag antibody, and LDHA mRNA abundance in the immunoprecipitated fraction was measured by qRT-PCR. **H,** The relative enrichment of IGF2BP2 in the 3′UTR of LDHA mRNA was detected by RIP assays in *circARHGAP29*-OE PC3 cells and in *circARHGAP29*-KD PC3/DR cells. **I,** The LDHA 3′UTR reporter constructs containing WT or mutant IGF2BP2 binding motif were cotransfected with control siRNA, siIGF2BP2 #1, or si*circARHGAP29* #1 cells in PC3 cells. The luciferase activities were measured using a dual luciferase reporter assay kit. **J,** The mRNA expression of LDHA was measured by qRT-PCR in PC3/DR cells after transfection with siIGF2BP2 #1 or si*circARHGAP29* #1 upon ActD treatment for 8 hours. **K,** qRT-PCR assay was used to detect the expression of LDHA in *circARHGAP29*-KD PC3/DR cells after transfection with IGF2BP2 WT or deletion mutant (Del) plasmids. The data are presented as the mean ± SD of at least three independent experiments. *, $P < 0.05$.

circARHGAP29 promotes LDHA expression by stabilizing the c-Myc level

A recent study demonstrated that IGF2BP2 could regulate c-Myc expression by recognizing the m6A modification in thyroid cancer (22). Consistent with the above results of *LDHA* mRNA, we also found that *circARHGAP29* could stabilize *c-Myc* mRNA by binding to the IGF2BP2 protein (**Fig. 6A** and **B**). Interestingly, we further identified that *circARHGAP29* could bind to the c-Myc protein by pulldown and RIP assays (**Fig. 6C** and **D**). To identify which region of the c-Myc protein interacts with *circARHGAP29*, PC3/DR cells were

transfected with plasmids expressing various fragments of the c-Myc (**Fig. 6E**). As shown in **Fig. 6F**, fragment 3 of Flag-tagged c-Myc plasmids interacted with *circARHGAP29*, which matched the predicted binding sites by the bioinformatic website catRAPID (Supplementary Fig. S6A). Inhibition of *circARHGAP29* decreased the protein level of c-Myc, while OE of *circARHGAP29* increased the c-Myc protein level (**Fig. 6G**). Given these observations, we hypothesized that *circARHGAP29* also regulated c-Myc levels posttranscriptionally. Thus, we speculated whether *circARHGAP29* could protect c-Myc from degradation. To assess this possibility, PC3 cells were treated with the protein synthesis inhibitor cycloheximide or the proteasome inhibitor bortezomib. As shown in **Fig. 6H**, ectopic expression of *circARHGAP29* inhibited the degradation of c-Myc proteins in the presence of cycloheximide. In contrast, bortezomib treatment reversed the decreased protein level of c-Myc induced by *circARHGAP29* KD (**Fig. 6I**). Collectively, these data indicated that *circARHGAP29* promoted the mRNA and protein expression of c-Myc in prostate cancer cells. Previous studies have shown that c-Myc could bind to the promoter of LDHA to promote LDHA expression (23, 24). Under these circumstances, we speculated that *circARHGAP29* could also activate LDHA expression through c-Myc activation. Inhibition of *circARHGAP29* decreased the mRNA expression of *LDHA*, which could be reversed by c-Myc OE (**Fig. 6J**). In addition, ChIP-qPCR assays also confirmed that KD of *circARHGAP29* inhibited the binding efficiency of c-Myc in the promoter of LDHA (**Fig. 6K**). We next detected the effect of *circARHGAP29* on the transcriptional activity of the LDHA gene by luciferase assay. KD of *circARHGAP29* impaired the transcriptional level of the LDHA promoter in PC3/DR cells (**Fig. 6L**). In addition, FISH-IF assays showed that KD of *circARHGAP29* inhibited the c-Myc expression and nuclear translocation to further restrain its transcriptional function (**Fig. 6M**). In *in vivo* experiments, IHC staining showed that inhibition of *circARHGAP29* decreased the protein level of c-Myc and LDHA (**Fig. 6N**). Besides, we also found that the expression of c-Myc was upregulated in primary prostate cancer samples compared with their adjacent tissues, and elevated expression of c-Myc was positively correlated with *circARHGAP29* level in patients with prostate cancer (**Fig. 6O** and **P**). Together, these data suggest that *circARHGAP29* could promote the expression of LDHA by stabilizing the c-Myc mRNA and protein levels.

CircARHGAP29 promotes LDHA-mediated glycolysis through the IGF2BP2/c-Myc pathway

Given the above-revealed molecular mechanisms by which *circARHGAP29* promotes LDHA expression by IGF2BP2/c-Myc signaling, we investigated the glycolytic phenotype upon *circARHGAP29* KD or OE. As expected, inhibition of *circARHGAP29* significantly decreased the docetaxel resistance and extracellular glucose consumption in PC3/DR cells (**Fig. 7A** and **B**) and 22RV1/DR cells under docetaxel treatment (Supplementary Fig. S7A and S7B). In addition, lactic acid production and LDH activities were also inhibited after *circARHGAP29* KD in PC3/DR cells (**Fig. 7C** and **D**) and 22RV1/DR cells after treatment with docetaxel (Supplementary Fig. S7C). In contrast, ectopic expression of *circARHGAP29* dramatically increased chemoresistance, glucose consumption, lactic acid production, and LDH activities in PC3 cells (**Fig. 7E–H**) and 22RV1 cells under docetaxel treatment (Supplementary Fig. S7D–S7F). To investigate whether *circARHGAP29* promoted docetaxel resistance through the promotion of aerobic glycolysis, we detected cell growth and glucose metabolism followed by LDHA inhibitor FX11 treatment in *circARHGAP29*-transfected prostate cancer cells. As expected, blocking glucose metabolism by FX11 significantly overrode the *circARHGAP29*-mediated docetaxel resistance and aerobic glycolysis (**Fig. 7E–H**; Supplementary Fig. S7D–S7F). Moreover, inhibition of LDHA by siRNA also resensitized PC3/DR and 22RV1/DR cells to docetaxel (Supplementary Fig. S7G and S7H). These data suggested that *circARHGAP29* desensitized prostate cancer cells to docetaxel treatment by activating glucose metabolism. Moreover, we also identified that OE of IGF2BP2 or c-Myc significantly rescued the *circARHGAP29*-KD–induced decrease in cell proliferation and lactic acid production (**Fig. 7I** and **J**; Supplementary Fig. S7I and S7J). In contrast, KD of IGF2BP2 or c-Myc expression dramatically blocked *circARHGAP29*-induced increases in cell growth and lactic acid production (**Fig. 7K** and **L**; Supplementary Fig. S7K and S7L). To further reveal the clinical relevance of *circARHGAP29* regulation in glycolysis in prostate cancer, we examined the expression of *circARHGAP29* and LDHA in a cohort of patients with prostate cancer. As shown in **Fig. 7M**, the expression levels of LDHA were significantly higher in the tumor tissues from these patients than in the matched paracancer tissues. Notably, upregulated expression of LDHA was positively correlated with the levels of *circARHGAP29* transcripts (**Fig. 7N**). In summary, these data indicate that *circARHGAP29*-regulated LDHA-induced glycolytic metabolism depends on IGF2BP2/c-Myc signaling (**Fig. 7O**).

Discussion

Herein, we revealed a potential role and regulatory mechanism of *circARHGAP29* in regulating docetaxel resistance of prostate cancer via IGF2BP2/c-Myc/LDHA signaling. Resistance to chemotherapeutic agents, either intrinsic or acquired, is currently one of the major challenges in the treatment of malignant disease. Until now, several factors have been associated with docetaxel resistance, including the expression of different isoforms of tubulin, activation of drug efflux pumps, PTEN loss, and activation of survival pathways (i.e., PI3K/AKT and mTOR and Notch2/Hedgehog signaling; refs. 3, 4). Otherwise, several circRNAs have been identified for prostate cancer progression and chemoresistance, presenting new perspectives for exploring molecular pathways (25). Due to their closed-loop structure, circRNAs are more resistant to degradation than linear RNAs, where they hold promise for utilization for cancer diagnosis, monitoring, prognosis, and prediction for therapeutic responsiveness (5, 6). In this study, we sought to search for aberrantly expressed circRNAs in docetaxel-resistant prostate cancer cells by RNA-seq analysis. At the beginning of this study, we chose three hormone-resistant prostate cancer cell lines (PC3, 22RV1, and DU145) to generate docetaxel-resistant cell lines by increasing the concentrations of docetaxel in a stepwise manner over 6 to 9 months (26). Among them, PC3 and DU145 cells are androgen receptor–negative cell lines, while 22RV1 cells are androgen receptor–positive cells. Subsequently, we identified that *circARHGAP29* was significantly upregulated in PC3/DR cells compared with PC3 cells by using RNA-seq, which was further confirmed by qRT-PCR assay, showing an over 5-fold increase of the circARHGAP29 expression in both PC3/DR and 22RV1/DR cells when compared with those of PC3 and 22RV1 cells. However, there was no significant change of circARHGAP29 levels between DU145/DR and DU145 cells, indicating other circRNAs may contribute to the docetaxel resistance of DU145 cells. Therefore, we chose PC3 and 22RV1 cells to further elucidate the potential role and mechanisms of *circARHGAP29* in docetaxel-resistant prostate cancer. In 2020, Shen and colleagues reported that *circFoxo3* inhibits LNCaP and DU145 cell growth, migration, invasion, and chemoresistance to

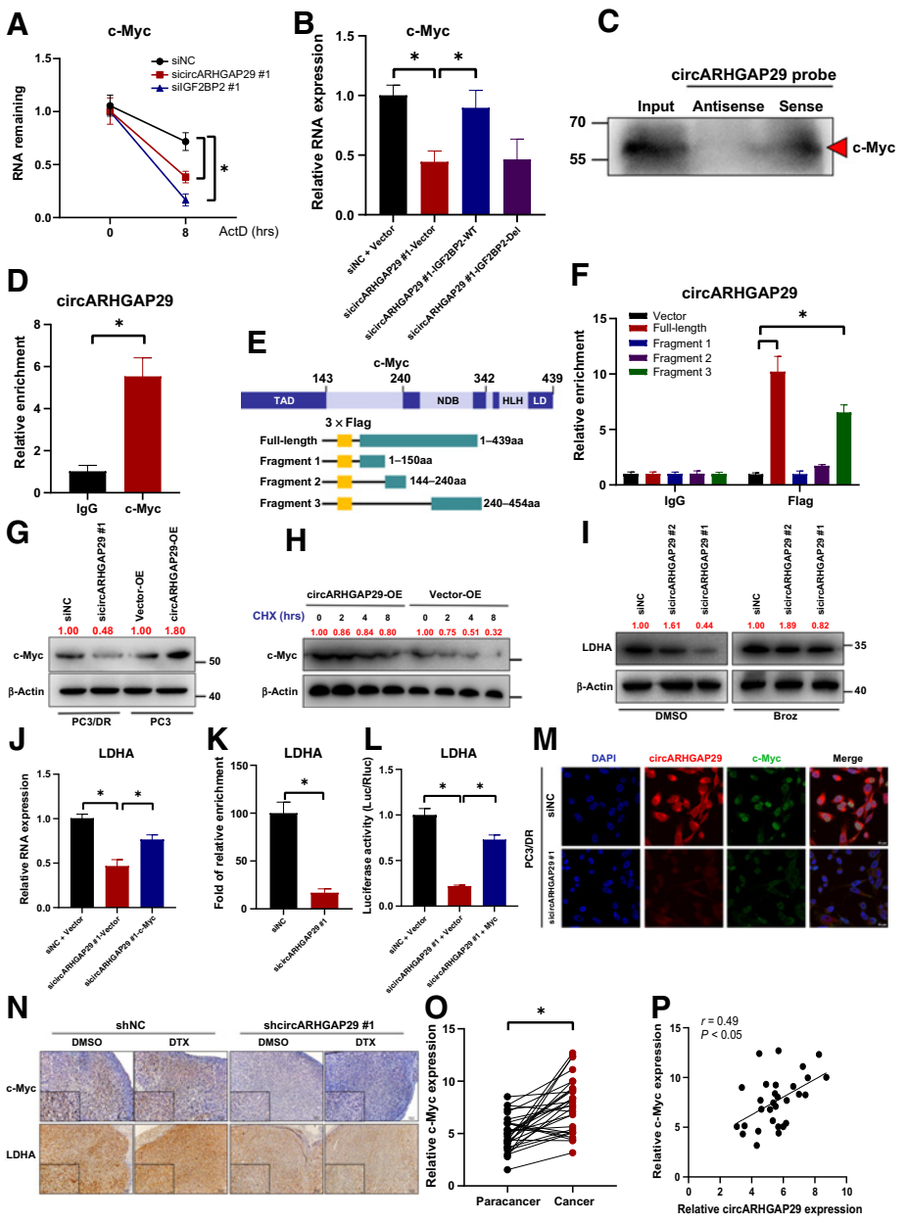

Figure 6.

circARHGAP29 promotes LDHA expression by stabilizing the c-Myc level. **A,** The mRNA expression of LDHA was analyzed by qRT-PCR in PC3/DR cells after transfection with siIGF2BP2 #1 or si*circARHGAP29* #1 upon ActD treatment for 8 hours. **B,** qRT-PCR analysis was used to detect the expression of c-Myc in *circARHGAP29*-KD PC3/DR cells after transfection with IGF2BP2 WT or deletion mutant plasmids. **C,** RNA pulldown assay and Western blot were performed to detect the association between c-Myc protein and *circARHGAP29*. **D,** RIP assay was performed using anti-IgG and anti–c-Myc antibodies, and specific primers were used to detect *circARHGAP29* by qRT-PCR. **E,** Identification of the c-Myc protein regions that interact with *circARHGAP29*. The different fragment plasmids of the c-Myc protein are illustrated at bottom. **F,** The interaction of c-Myc protein regions with *circARHGAP29* in PC3 cells was determined by using a RIP assay. **G,** Western blot was used to evaluate the protein level of c-Myc upon *circARHGAP29* OE or KD. **H,** The effect of protein synthesis inhibitor cycloheximide (CHX) treatment on the change in the c-Myc protein level mediated by *circARHGAP29* OE as detected by Western blot. **I,** Western blot was used to evaluate the change of c-Myc protein in *circARHGAP29*-KD PC3/DR cells upon proteasome inhibitor bortezomib (Borz) treatment. ImageJ was used to compare the density of bands on Western blot. **J,** The relative mRNA expression of LDHA was detected by qRT-PCR in *circARHGAP29*-KD PC3/DR cells after transfection with c-Myc expression plasmids. **K,** ChIP-qPCR shows the binding efficiency of c-Myc to the LDHA gene promoter. **L,** The luciferase activities were measured in *circARHGAP29*-KD PC3/DR cells with either c-Myc plasmids or vectors. **M,** The intracellular location of c-Myc and *circARHGAP29* in PC3/DR cells after *circARHGAP29* KD was detected by FISH-IF assay. **N,** IHC staining showed the expression of c-Myc and LHDA in *circARHGAP29*-KD tumors and their control tissues upon docetaxel (DTX) or DMSO treatment. **O,** The c-Myc expression was evaluated by qRT-PCR in primary prostate cancer samples and paracancer tissues. **P,** The correlation between *c-Myc* and *circARHGAP29* in clinical prostate cancer samples was assessed by the Spearman correlation analysis. The data are presented as the mean ± SD of at least three independent experiments. *, $P < 0.05$.

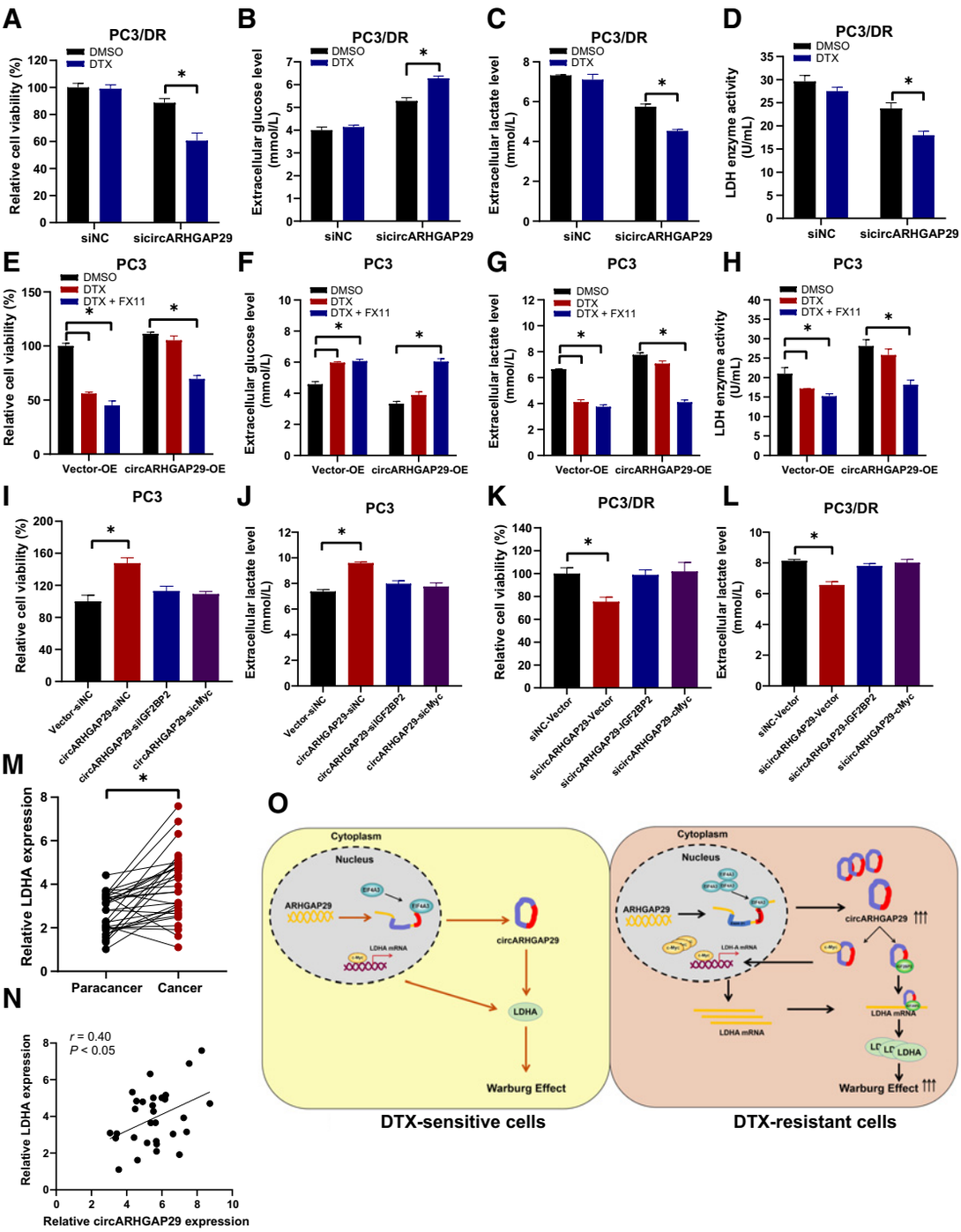

Figure 7.

CircARHGAP29 promotes LDHA-mediated glycolysis through the IGF2BP2/c-Myc pathway. **A,** Cell viability was measured by CCK-8 assay in *circARHGAP29*-KD PC3/DR cells upon docetaxel (DTX) treatment. **B–D,** The extracellular glucose concentration, lactic acid level, and LDH activities were detected in *circARHGAP29*-KD PC3/DR cells after docetaxel treatment. **E–H,** The docetaxel resistance, extracellular glucose content, lactic acid level, and LDH activities were detected in *circARHGAP29*-OE PC3 cells under docetaxel and/or LDHA inhibitor FX11 treatment. **I** and **J,** Cell growth and lactic acid level were analyzed in *circARHGAP29*-OE PC3 cells after transfection with si-IGF2BP2 #1, si-c-Myc #1, or control siRNA. **K** and **L,** Cell proliferation assay and lactic acid level were evaluated in *circARHGAP29*-KD PC3/DR cells transfected with IGF2BP2 or c-Myc plasmids. **M,** The relative expression of LDHA was measured by qRT-PCR in 30 pairs of clinical prostate cancer samples. **N,** The positive relation between *circARHGAP29* and LDHA in clinical samples by qRT-PCR. **O,** The schematic diagram shows that EIF4A3-induced *circARHGAP29* promotes the aerobic glycolysis in docetaxel-resistant prostate cancer through IGF2BP2/c-Myc/LDHA signaling. The data are presented as the mean ± SD of at least three independent experiments. *, $P < 0.05$.

docetaxel by promoting the expression of its parent gene Foxo3 (27). In addition, inhibition of *hsa_circ_0000735* promoted docetaxel sensitivity and impeded the malignant behaviors of docetaxel-resistant PC3 and DU145 cells by sponging miR-7 (28). Moreover, Ding and colleagues further identified that circ_0057558 promotes cell proliferation, cell cycle transition, and docetaxel resistance of 22RV1 and DU145 cells. Mechanistic studies indicated that *circ_0057558* could sequester miR-206 and liberate the transcription of its target gene USP33 and thus deubiquitinate c-Myc (29). Recently, Zhang and colleagues also found that exosomal *circ-XIAP* promotes docetaxel resistance in PC3 and DU145 cells by regulating the miR-1182/TPD52 axis (30). In this study, we found that ectopic expression of *circARHAP29* in PC3 and 22RV1 cells promotes cell growth and docetaxel resistance, whereas inhibition of *circARHAP29* resensitive PC3/DR and 22RV1/DR cells to docetaxel. Besides, elevated expression of *circARHGAP29* was associated with higher Gleason score and clinical tumor stage in patients with localized prostate cancer, and worse response to docetaxel chemotherapy in patients with metastatic prostate cancer.

Previous studies have indicated that RBPs play an important role in the formation of circRNAs (18). EIF4A3 functions as an RBP mainly localized in the nucleus and is a core component of the exon junction complex and is widely involved in RNA splicing and nonsense-mediated mRNA decay (19, 31). Recent studies have shown that EIF4A3 facilitates *circSEPT9* and *circASAP1* expression by binding to their parental pre-mRNA transcript (32, 33). In the current study, we found that the cytoplasmic expression of EIF4A3 and *circARHGAP29* were greatly upregulated in docetaxel-resistant prostate cancer cells. Moreover, we further confirmed that EIF4A3 could combine with the back-spliced junction site and the downstream flanking sequences of *circARHGAP29* pre-mRNA by the 161–212 aa binding sites of EIF4A3. By using gain- and loss-of-function experiments, we identified that EIF4A3 could promote the expression and cyclization of *circARHGAP29*. Besides, nuclear/cytoplasmic fraction assay revealed that EIF4A3 KD inhibits the cytoplasmic export of *circARHGAP29*. Therefore, the above data together demonstrate the critical role of *circARHGAP29* in docetaxel-resistant prostate cancer cells and elucidate the mechanism of how *circARHGAP29* was upregulated by EIF4A3. Nevertheless, the specific mechanism by how EIF4A3 mediates the cytoplasmic export of *circARHGAP29* in docetaxel-resistant prostate cancer cells should be further investigated (34).

To further explore the therapeutic function in docetaxel-resistant prostate cancer, we predicted the biological characteristics of *circARHGAP29* by using the online database. Regarding the regulatory mechanisms of circRNAs, several studies have demonstrated that cytoplasmic circRNAs mainly participate in regulating protein stability and modification. In our study, we found that *circARHGAP29* does not have the ability to bind to Ago2; therefore, it is ruled out as a miRNA sponge. In addition, we further excluded the protein- or peptide-encoding features of *circARHGAP29* after circRNADb database analysis. Subsequently, we analyzed the *circARHGAP29* interacting protein through RNA pulldown experiments using a specific biotin-labeled probe. Following silver staining, we found several specific bands with molecular weights of 55 to 70 kDa in the *circARHGAP29* probe group, which were ultimately identified as IGF2BP2 by mass spectrometry analysis and Western blotting. Consistent with the above data, the circAltas database also predicted that IGF2BP2 ranks at the top among the *circARHGAP29*-related RBPs. Besides, we did not find the interaction between IGF2BP2 and EIF4A3 protein by coimmunoprecipitation assay. Previous studies indicated that IGF2BP2 is critical for posttranscriptional gene expression regulation to coordinate cellular function and nutrient metabolisms, such as glucose tolerance and insulin sensitivity (20, 21). Herein, we found that LDHA is the target of both *circARHGAP29* and IGF2BP2 based on RNA-seq and CLIP-seq data. Further studies demonstrated that *circARHGAP29* could promote the mRNA stability of LDHA through the formation of a *circARHGAP29*/IGF2BP2/*LDHA* RNA-protein ternary complex.

Emerging studies have indicated that metabolic adaptations of cancer cells have been linked to their resistance to chemotherapeutics, such as glycolysis, lipid metabolism, and polyamine synthesis (35). Elevated glycolytic activity insures that adequate ATP levels are available to meet the demands of ATP-binding cassette transporters to mediate drug efflux and confer resistance to chemotherapy. Besides, excessive lactic acid production by aerobic glycolysis is strictly associated with the stemness of cancer cells, which further mediates chemoresistance (36). Targeting LDHA promotes docetaxel-induced cytotoxicity predominantly in castration-resistant prostate cancer cells (37). Besides, several studies have revealed that circRNAs can regulate the cancer metabolism process by affecting the expression of glycolysis-relevant enzymes and pathways (38). In this study, we found that *circARHGAP29* could promote LDHA-mediated cell proliferation and glycolysis in docetaxel-resistant prostate cancer cells by binding to the IGF2BP2 protein. Furthermore, previous studies demonstrated that c-Myc bound to the promoter regions of LDHA to activate transcription (23, 24). Consistent with the above LDHA results, we found that the mRNA level of *c-Myc* could be upregulated by the *circARHGAP29*/IGF2BP2 complex. Surprisingly, we also found that *circARHGAP29* directly interacts with and stabilizes the c-Myc protein, thus increasing LDHA transcription and ultimately activating glycolytic metabolism. These combined results indicate that *circARHGAP29* promotes LDHA-induced aerobic glycolysis in docetaxel-resistant prostate cancer cells through interacting with IGF2BP2 and c-Myc. However, the degradation pathways of c-Myc in *circARHGAP29*-induced chemoresistance in prostate cancer are still largely unknown and should be further elucidated (39).

In summary, we identified a novel circRNA, *circARHGAP29*, that was upregulated in docetaxel-resistant prostate cancer cell lines and clinical samples, and we also found that elevated expression of *circARHGAP29* could effectively promote prostate cancer cell proliferation, docetaxel resistance, and glucose metabolism. Mechanistically, we first discovered that *circARHGAP29* mediated by EIF4A3 directly binds to IGF2BP2, thereby contributing to stabilizing LDHA mRNA levels. Moreover, *circARHGAP29* could also interact and stabilize the mRNA and protein expression of c-Myc, which activates LDHA expression by facilitating its transcription. Our findings demonstrate that *circARHGAP29* could be a critical prognostic biomarker and promising therapeutic target in docetaxel-resistant prostate cancer.

Authors' Disclosures

No disclosures were reported.

Authors' Contributions

X. Jiang: Conceptualization, data curation, formal analysis, funding acquisition, investigation, visualization, methodology, writing–original draft. **S. Guo:** Formal analysis, funding acquisition, investigation, methodology, writing–review and editing. **S. Wang:** Formal analysis, validation, investigation. **Y. Zhang:** Data curation, formal analysis, validation, investigation, methodology. **H. Chen:** Conceptualization, validation, investigation. **Y. Wang:** Investigation, methodology. **R. Liu:** Investigation, methodology. **Y. Niu:** Formal analysis, supervision, writing–review and editing.

Y. Xu: Conceptualization, resources, supervision, funding acquisition, validation, writing–original draft, project administration, writing–review and editing.

Acknowledgments

This work was funded by grants from the National Natural Science Foundation of China (81802568 and 82174174), the Bilateral Inter-Governmental S&T Cooperation Project from Ministry of Science and Technology of China (2018YFE0114300), the Tianjin Municipal Science and Technology Project (20JCQNJC00530), and the Tianjin Health Science and Technology Project (KJ20169). The authors thank Professor Jie Hong (Shanghai Institute of Digestive Disease, Shanghai Jiao Tong University) for kindly providing the primer sequences of ChIP-qPCR.

The costs of publication of this article were defrayed in part by the payment of page charges. This article must therefore be hereby marked *advertisement* in accordance with 18 U.S.C. Section 1734 solely to indicate this fact.

Received September 3, 2021; revised November 15, 2021; accepted December 21, 2021; published first December 28, 2021.

Reference

1. Siegel RL, Miller KD, Fuchs HE, Jemal A. Cancer statistics, 2021. CA Cancer J Clin 2021;71:7–33.
2. Cornford P, van den Bergh RCN, Briers E, Van den Broeck T, Cumberbatch MG, De Santis M, et al. EAU-EANM-ESTRO-ESUR-SIOG guidelines on prostate cancer. Part II-2020 update: treatment of relapsing and metastatic prostate cancer. Eur Urol 2021;79:263–82.
3. Seruga B, Ocana A, Tannock IF. Drug resistance in metastatic castration-resistant prostate cancer. Nat Rev Clin Oncol 2011;8:12–23.
4. Rizzo M. Mechanisms of docetaxel resistance in prostate cancer: the key role played by miRNAs. Biochim Biophys Acta Rev Cancer 2021;1875:188481.
5. Zhou WY, Cai ZR, Liu J, Wang DS, Ju HQ, Xu RH. Circular RNA: metabolism, functions, and interactions with proteins. Mol Cancer 2020;19:172.
6. Ma S, Kong S, Wang F, Ju S. CircRNAs: biogenesis, functions, and role in drug-resistant tumors. Mol Cancer 2020;19:119.
7. Chen S, Huang V, Xu X, Livingstone J, Soares F, Jeon J, et al. Widespread and functional RNA circularization in localized prostate cancer. Cell 2019;176:831–43.
8. Vo JN, Cieslik M, Zhang Y, Shukla S, Xiao L, Zhang Y, et al. The landscape of circular RNA in cancer. Cell 2019;176:869–81.
9. Kim J, DeBerardinis RJ. Mechanisms and implications of metabolic heterogeneity in cancer. Cell Metab 2019;30:434–46.
10. Feng Y, Xiong Y, Qiao T, Li X, Jia L, Han Y. Lactate dehydrogenase A: a key player in carcinogenesis and potential target in cancer therapy. Cancer Med 2018;7:6124–36.
11. Lin J, Xia L, Liang J, Han Y, Wang H, Oyang L, et al. The roles of glucose metabolic reprogramming in chemo- and radioresistance. J Exp Clin Cancer Res 2019;38:218.
12. Ma L, Zong X. Metabolic symbiosis in chemoresistance: refocusing the role of aerobic glycolysis. Front Oncol 2020;10:5.
13. Sun H, Wang H, Wang X, Aoki Y, Wang X, Yang Y, et al. Aurora-A/SOX8/FOXK1 signaling axis promotes chemoresistance via suppression of cell senescence and induction of glucose metabolism in ovarian cancer organoids and cells. Theranostics 2020;10:6928–45.
14. Zhou M, Zhao Y, Ding Y, Liu H, Liu Z, Fodstad O, et al. Warburg effect in chemosensitivity: targeting lactate dehydrogenase A resensitizes taxol-resistant cancer cells to taxol. Mol Cancer 2010;9:33.
15. Han JH, Kim M, Kim HJ, Jang SB, Bae SJ, Lee IK, et al. Targeting lactate dehydrogenase A with catechin resensitizes SNU620/5FU gastric cancer cells to 5-Fluorouracil. Int J Mol Sci 2021;22:5406.
16. Jiang X, Guo S, Zhang Y, Zhao Y, Li X, Jia Y, et al. LncRNA NEAT1 promotes docetaxel resistance in prostate cancer by regulating ACSL4 via sponging miR-34a-5p and miR-204-5p. Cell Signal 2020;65:109422.
17. Domingo-Domenech J, Vidal SJ, Rodriguez-Bravo V, Castillo-Martin M, Quinn SA, Rodriguez-Barrueco R, et al. Suppression of acquired docetaxel resistance in prostate cancer through depletion of notch- and hedgehog-dependent tumor-initiating cells. Cancer Cell 2012;22:373–88.
18. Welden JR, Stamm S. Pre-mRNA structures forming circular RNAs. Biochim Biophys Acta Gene Regu Mech 2019;1862:194410.
19. Chan CC, Dostie J, Diem MD, Feng W, Mann M, Rappsilber J, et al. eIF4A3 is a novel component of the exon junction complex. RNA 2004;10:200–9.
20. Dai N. The diverse functions of IMP2/IGF2BP2 in metabolism. Trends Endocrinol Metab 2020;31:670–9.
21. Bell JL, Wächter K, Mühleck B, Pazaitis N, Köhn M, Lederer M, et al. Insulin-like growth factor 2 mRNA-binding proteins (IGF2BP): posttranscriptional drivers of cancer progression? Cell Mol Life Sci 2013;70:2657–75.
22. Huang H, Weng H, Sun W, Qin X, Shi H, Wu H, et al. Recognition of RNA N6-methyladenosine by IGF2BP proteins enhances mRNA stability and translation. Nat Cell Biol 2018;20:285–95.
23. Shim H, Dolde C, Lewis BC, Wu CS, Dang G, Jungmann RA, et al. c-Myc transactivation of LDHA: implications for tumor metabolism and growth. Proc Natl Acad Sci U S A 1997;94:6658–63.
24. Dang CV, Le A, Gao P. MYC-induced cancer cell energy metabolism and therapeutic opportunities. Clin Cancer Res 2009;15:6479–83.
25. Xu T, Wang M, Jiang L, Ma L, Wan L, Chen Q, et al. CircRNAs in anticancer drug resistance: recent advances and future potential. Mol Cancer 2020;19:127.
26. O'Neill AJ, Prencipe M, Dowling C, Fan Y, Mulrane L, Gallagher WM, et al. Characterization and manipulation of docetaxel-resistant prostate cancer cell lines. Mol Cancer 2011;10:126.
27. Shen Z, Zhou L, Zhang C, Xu J. Reduction of circular RNA Foxo3 promotes prostate cancer progression and chemoresistance to docetaxel. Cancer Lett 2020;468:88–101.
28. Gao Y, Liu J, Huan J, Che F. Downregulation of circular RNA hsa_circ_0000735 boosts prostate cancer sensitivity to docetaxel via sponging miR-7. Cancer Cell Int 2020;20:334.
29. Ding T, Zhu Y, Jin H, Zhang P, Guo J, Zheng J. Circular RNA circ_0057558 controls prostate cancer cell proliferation through regulating miR-206/USP33/c-Myc axis. Front Cell Dev Biol 2021;9:644397.
30. Zhang H, Li M, Zhang J, Shen Y, Gui Q. Exosomal circ-XIAP promotes docetaxel resistance in prostate cancer by regulating miR-1182/TPD52 axis. Drug Des Devel Ther 2021;15:1835–49.
31. Zhu Y, Ren C, Yang L. Effect of eukaryotic translation initiation factor 4A3 in malignant tumors. Oncol Lett 2021;21:358.
32. Wei Y, Lu C, Zhou P, Zhao L, Lyu X, Yin J, et al. EIF4A3-induced circular RNA ASAP1 promotes tumorigenesis and temozolomide resistance of glioblastoma via NRAS/MEK1/ERK1–2 signaling. Neuro Oncol 2021;23:611–24.
33. Zheng X, Huang M, Xing L, Yang R, Wang X, Jiang R, et al. The circRNA circSEPT9 mediated by E2F1 and EIF4A3 facilitates the carcinogenesis and development of triple-negative breast cancer. Mol Cancer 2020;19:73.
34. Li Z, Kearse MG, Huang C. The nuclear export of circular RNAs is primarily defined by their length. RNA Biol 2019;16:1–4.
35. Chen X, Chen S, Yu D. Metabolic reprogramming of chemoresistant cancer cells and the potential significance of metabolic regulation in the reversal of cancer chemoresistance. Metabolites 2020;10:289.
36. Tyagi K, Mandal S, Roy A. Recent advancements in therapeutic targeting of the Warburg effect in refractory ovarian cancer: a promise towards disease remission. Biochim Biophys Acta Rev Cancer 2021;1876:188563.
37. Muramatsu H, Sumitomo M, Morinaga S, Kajikawa K, Kobayashi I, Nishikawa G, et al. Targeting lactate dehydrogenase-A promotes docetaxel-induced cytotoxicity predominantly in castration-resistant prostate cancer cells. Oncol Rep 2019;42:224–30.
38. Li T, Xian HC, Dai L, Tang YL, Liang XH. Tip of the iceberg: roles of circRNAs in cancer glycolysis. OncoTargets Ther 2021;14:2379–95.
39. Tu R, Chen Z, Bao Q, Liu H, Qing G. Cross-talk between oncogenic MYC and noncoding RNAs in cancer. Semin Cancer Biol 2021;75:62–71.